

# Holons in chiral spin liquids: statistics and pairing

D.M. Deaven, D.S. Rokhsar

*Department of Physics, University of California, Berkeley, CA 94720*

A. Barbieri

*Lawrence Berkeley Laboratory, Berkeley, CA 94720*

(November 16, 2018)

We study Gutzwiller-projected variational wavefunctions for charged, spinless holon excitations in chiral spin liquids. We find that these states describe anyons, with a statistical phase  $\Phi_s$  that is continuously adjustable between 0 and  $\pi/2$ , depending on a variational parameter. The statistical flux attached to each holon is localized to within a lattice constant. By diagonalizing the effective Hamiltonian for charge motion in our variational basis we obtain a two-holon pair state. This two-holon state has large overlap with a two-hole state whose relative wavefunction has  $d$ -wave symmetry and breaks time-reversal and parity.

## I. INTRODUCTION

The notion of a quasiparticle is a remarkably successful organizing principle for understanding many-body systems. In strongly interacting Fermi systems such as  $^3\text{He}$ , for example, many-body effects simply renormalize the mass and interactions of the Landau quasiparticles; their charge, spin, and statistics the same as those of the bare atoms.<sup>1</sup> Other many-body systems, however, possess low-energy charged excitations that are dramatically different from Landau quasiparticles. In the fractional quantum Hall effect, for example, a large magnetic field and the Coulomb repulsion between electrons conspire to produce Laughlin quasiparticles with fractional charge and statistics.<sup>2</sup> In *trans*-polyacetylene, a system with broken translational symmetry, charges bind to domain walls, forming soliton excitations with charge  $e$  but without spin.<sup>3</sup> In both of these cases, the novel quasiparticles have a “topological” character, because they cannot be created by local combinations of bare electron creation and destruction operators, in contrast with Landau quasiparticles. Nevertheless, these unconventional quasiparticles are well defined, weakly interacting objects which describe the low-energy states of the many-body system.

Similarly, unconventional quasiparticles have been suggested as the charge carriers in “resonating valence bond” theories of high temperature superconductivity.<sup>4,5,6</sup> Motivated by the fact that cuprate high temperature superconductivity arises upon doping antiferromagnets exhibiting large quantum fluctuations, these theories focus on spin-1/2 systems with local antiferromagnetic correlations but no long range order – so-called “spin liquids.”

The phase diagram of the high temperature superconductors motivates the study of spin liquids as a stepping stone in a novel approach to the superconducting state. Referring to fig. 1, the real materials reside in

the temperature-doping plane; an additional axis, labeled frustration, is added for theoretical convenience. When the parent insulators are doped, antiferromagnetic long range order is destroyed almost simultaneously with the onset of superconducting order. (A “spin glass” regime due to disorder may intervene.) It is appealing to try to separate the effects of loss of magnetic order from the instability to superconductivity. In principle, this could be accomplished theoretically by first introducing fictitious frustrating interactions in the antiferromagnetic insulator, thereby destroying long range order without introducing charge carriers. Then, to study the appearance of superconductivity, this “spin liquid” state would be doped, so that one could consider the motion of dilute charge carriers in a spin background resembling the fluctuating spins in the real materials’ superconducting state.

Finally, to return the theory to a more realistic model of the actual copper oxide planes, the fictitious frustrating interactions would be turned off – they would be no longer needed, since magnetic frustration is implicitly generated by charge carrier motion.<sup>7</sup> In this roundabout manner, one would arrive at a description of the real materials’ superconducting state. Assuming that no phase transition intervenes, the superconducting state achieved upon doping the spin liquid would have the same symmetry and general features as the real superconducting state. This approach contrasts the more direct “BCS approach,” which begins from an understanding of the normal metal at high temperature (which may be problematic in the cuprates) and then considers residual attractive interactions between quasiparticles. If properly executed, both the spin liquid and the BCS approaches should arrive at the same superconducting state, but from different directions.

Unfortunately for the spin liquid approach, it has proven difficult to find suitably frustrated spin mod-

FIG. 1. Schematic phase diagram for high temperature superconductivity. The real materials occupy the temperature-doping plane; an additional axis, labeled frustration, is included for theoretical convenience. In a BCS-like approach, the superconducting state is entered from a well understood normal state. In the “resonating-valence-bond” or “spin liquid” approach, a disordered quantum antiferromagnet is stabilized by artificially adding magnetic frustration to the undoped parent compound. This spin liquid is then doped to form a superconductor. The condensate is formed from bound holon pairs, the charge carrying quasiparticles in a doped spin-liquid. If no phase transition intervenes as the frustration is turned off in the doped state, both the spin liquid and BCS approaches must arrive at the same superconducting state, but from complementary physical points of view.

els which destroy antiferromagnetic order without introducing additional unwanted broken symmetry ground states. There is no short-ranged spin model known to have a spin liquid ground state. Nevertheless, spin liquids may be usefully thought of as metastable phases of frustrated antiferromagnets that mimic the spin correlations of cuprate superconductors, even if they are not the true ground state of a particular frustrated spin system. One can still study their excitation spectra, and hope to carry out the program outlined above. In this work we consider simple variational “chiral spin liquid” states<sup>8</sup> which break time-reversal and parity symmetries but are translationally invariant. They have good variational energies for simple frustrated spin Hamiltonians, and suggest natural variational states when doped. By studying the motion of a few charge carriers, we develop a scenario for understanding superconductors with broken time-reversal and parity symmetry.

We consider the  $t$ - $J$ - $J'$  Hamiltonian  $\mathcal{H} = \mathcal{H}_{\text{spin}} + \mathcal{H}_{\text{hop}}$ , where the first term is the (frustrated) spin Hamiltonian

$$\mathcal{H}_{\text{spin}} = \sum_{\langle ij \rangle} J_{ij} \mathbf{S}_i \cdot \mathbf{S}_j, \quad (1)$$

with first and second neighbor antiferromagnetic couplings  $J$  and  $J'$ , and the second term is the nearest-neighbor hopping Hamiltonian

$$\mathcal{H}_{\text{hop}} = -t \sum_{\langle ij \rangle, \sigma} c_{i\sigma}^\dagger c_{j\sigma}. \quad (2)$$

In these expressions  $c_{i\sigma}^\dagger$  creates a fermion at site  $i$  with spin projection  $\sigma$  and  $\mathbf{S}_i \equiv c_{i\alpha}^\dagger \boldsymbol{\sigma}_{\alpha\beta} c_{i\beta}$  is the spin operator at site  $i$ . Both Eqs. (1) and (2) are allowed to act only within the subspace of states in which no lattice site is doubly occupied.

In this work we address (a) the internal structure of charged “holon” excitations in a locally stable spin-liquid and (b) the dynamics and statistics of a dilute gas of these excitations. Sections II and III contain a brief general discussion of spin liquids and holon excitations and describe the specific wavefunctions we consider. Our main results are presented in sections IV and V. A brief summary is provided in section VI.

## II. CHIRAL SPIN LIQUIDS

Spin liquids are quantum antiferromagnets whose Néel order has been destroyed by large zero-point fluctuations of the interacting spins. These large quantum effects preclude the use of a spin-wave expansion about an ordered state. Instead, we appeal to the variational principle and take advantage of qualitative similarities between spin liquid states and certain simple Slater determinant states of spin-1/2 fermions. In particular, consider Slater determinant states  $|\chi\rangle$  which (a) are translationally invariant with an average density of one fermion per site, (b) have no average magnetic moment at each site, and (c) have spin and charge correlations which decay exponentially. All three of these properties are shared by spin liquids. The main difference between  $|\chi\rangle$  and a spin liquid is simply one of degree – a spin liquid has no number fluctuations at all, while  $|\chi\rangle$  has local number fluctuations.

This distinguishing property of  $|\chi\rangle$  can be eliminated by applying the complete Gutzwiller projector

$$P_G \equiv \prod_i (1 - n_{i\uparrow} n_{i\downarrow}), \quad (3)$$

which annihilates all configurations containing doubly-occupied sites. What remains is a superposition of spin configurations whose amplitudes are inherited from the original “pre-projected” Slater determinant. If this pre-projected state has short-ranged spin and charge correlations, then Gutzwiller projection is a “local” procedure.<sup>9</sup> The correlations in the projected state then closely follow the correlations of the pre-projected determinant, up to simple renormalization factors of order unity.<sup>10,11,12</sup>

It is surprisingly difficult to construct Slater determinants with the three properties listed above. To obtain a translationally invariant free-particle state with only short-range correlations, one should completely fill

FIG. 2. Schematic of a tight binding model  $H_\chi$  which breaks time-reversal and parity symmetries. Circles represent sites; lines represent hopping matrix elements between sites. A line with an arrow has phase  $\pi/4$  in the sense given by the arrow, a dashed line has phase  $\pi$ , and a solid line zero phase. (a) The flux state. Each elementary plaquette has  $\pi$  flux piercing it. (b) The chiral state. Each elementary triangle has flux  $\pi/2$  piercing it. Up to a gauge transformation, these tight-binding Hamiltonians are translationally invariant.

a band of single-particle states while simultaneously ensuring that a gap exists between the filled band and the next highest energy band. For a translationally invariant system, the resulting charge density will be uniform. The difficulty arises in constructing a translationally invariant system with a one-body energy gap. The simplest way to accomplish this is to consider particles moving on a lattice in a uniform commensurate (fictitious) magnetic field which couples only to orbital motion.<sup>8,13</sup> For appropriate field strength, the effective unit cell is doubled, and a gap is opened at half-filling. The hopping matrix elements will now be complex; as long as the net phase factor in the product of the elements around any closed loop is invariant under translations, the model ground state will also be translationally invariant, up to an overall gauge transformation.

FIG. 3. Single-particle bands of Eq. (4) in the two-site Square  $\sqrt{2} \times \sqrt{2}$  magnetic unit cell shown by the dotted line in the inset, with no background magnetic field (dashed line) and in the presence of a translationally invariant chiral field (solid line) as illustrated in fig. 2. Note that a gap equal to  $4m_0$  is opened at half-filling (filling the lower band).

In particular, let  $|\chi\rangle$  be the half-filled ground state of the square-lattice tight-binding Hamiltonian<sup>8</sup>

$$H_\chi = \sum_{ij\sigma} \chi_{ij} c_{i\sigma}^\dagger c_{j\sigma} \quad (4)$$

illustrated in fig. 2. Here  $\chi_{ij}$  is a complex link variable and  $c_{i\sigma}^\dagger$  creates a fermion at site  $i$  with spin projection  $\sigma$ . We arrange for a net phase  $\pi$  around every plaquette, and phase  $\pi/2$  around every elementary triangle (encircled clockwise, say). More explicitly, the complex product  $\chi_{AB}\chi_{BC}\chi_{CD}\chi_{DA}$  around any elementary plaquette  $ABCD$  has phase  $\pi$ , while the product  $\chi_{AB}\chi_{BC}\chi_{CA}$  around any elementary triangle  $ABC$  has phase  $\pi/2$ . We will refer to the phase around a closed loop a “flux,” since the (Aharonov-Bohm) phase for motion in a magnetic field is proportional to the flux enclosed by the path. One flux quantum  $hc/e$  corresponds to a phase  $2\pi$ .

The Hamiltonian Eq. (4) explicitly breaks both time-reversal and parity symmetries, each of which inverts the flux through every closed loop. In this work we shall set  $\chi_{ij} = 0$  for all but nearest and next-nearest neighboring sites  $i$  and  $j$ . We set  $|\chi_{ij}| = 1$  when sites  $i$  and  $j$  are nearest neighbors, and  $|\chi_{ij}| = m_0/2$  when sites  $i$  and  $j$  are next-nearest neighbors. This notation derives from the fact that for small values of  $m_0$  and at half filling, the noninteracting fermions whose motion is governed by Eq. (4) have a gap to excitations equal to  $4m_0$  (“mass,” in field-theory jargon). Figure 3 illustrates the gap opening due to the addition of the diagonal hopping strength  $m_0$ .

The similarity of the Gutzwiller-projected states  $P_G|\chi\rangle$  to the actual ground states of a doped antiferromagnet

may be measured by their variational energy. Consider  $\mathcal{H}$  with  $J_{ij} = J$  for nearest neighbor sites  $i$  and  $j$ , and  $J_{ik} = J'$  for next-nearest neighbor sites  $i$  and  $k$ . Then for each value of  $J'/J$  there is a corresponding value of  $m_0$  which minimizes the variational energy

$$E(J'/J; m_0) = \frac{\langle \chi | P_G \mathcal{H}_{\text{spin}}(J'/J) P_G | \chi \rangle}{\langle \chi | P_G | \chi \rangle} \Big|_{m_0}. \quad (5)$$

In this paper we study systems with values of  $m_0$  satisfying  $0 < m_0 \leq 1$ , which implicitly selects the value of  $J'/J$  via Eq. (5) (see ref. 12 for a more complete description of the properties of  $E(J'/J; m_0)$ ). For small  $J'$  it is generally believed<sup>14</sup> that the ground state of  $\mathcal{H}_{\text{spin}}$  has Néel order, unlike the variational states we consider here. For larger  $J'$  other more complicated types of broken symmetry ground states may be stabilized. For our purposes, we assume that the spin liquid states  $P_G | \chi \rangle$  are adequate models for the spin background of a lightly doped quantum antiferromagnet.

The parameter  $m_0$  plays a crucial role in our calculation. It corresponds to the gap in the spectrum of  $H_\chi$  at half-filling (see fig. 3) and determines the decay length  $\xi_\chi$  for exponentially decaying spin and charge correlations in the pre-projected state  $| \chi \rangle$ . For small  $m_0$ ,  $\xi_\chi \approx 1/m_0$ . (For general values of  $m_0$ ,  $\xi_\chi(m_0)$  has a more complicated but nonincreasing form<sup>12</sup> when  $0 < m_0 \leq 1$ .) The spin-spin correlation length in the *projected* state  $P_G | \chi \rangle$  is related to  $\xi_\chi$  by a numerical factor of order unity,<sup>12</sup> so  $m_0$  also adjusts the range of spin correlations in the fully projected state.

The introduction of a non-zero  $m_0$  in Eq. (4) breaks both T (time-reversal) and P (two-dimensional parity) symmetry.<sup>8</sup> This can be seen, for example, by computing the spin triple product  $\langle \mathbf{S}_i \cdot \mathbf{S}_j \times \mathbf{S}_k \rangle$  on any elementary triangle  $ijk$  in the projected state. This expectation value vanishes by symmetry when  $m_0$  vanishes, but is non-zero otherwise.

### III. SPINONS AND HOLONS

Unlike the creation of quasiparticles in a Fermi liquid, the creation of separated spin and charge excitations in spin liquids involves non-local operations. There are two schemes for producing holons and spinons in Gutzwiller projected states, which at first glance seem quite different.

*Scheme 1* – Anderson<sup>15</sup> begins with a locally non-neutral state of the form

$$c_{i-\sigma} c_{j\sigma'}^\dagger | \chi \rangle, \quad (6)$$

a Slater determinant to which a particle with spin projection  $\sigma'$  has been added at site  $j$  and a particle with spin projection  $-\sigma$  has been removed from site  $i$ . In this state,  $\langle n_j \rangle = 3/2$  and  $\langle n_i \rangle = 1/2$ , while  $\langle n_k \rangle = 1$  for all other sites  $k$ , as in the original Slater determinant state  $| \chi \rangle$ . The projected state

$$| i\sigma, j\sigma' \rangle \equiv P_G c_{i-\sigma} c_{j\sigma'}^\dagger | \chi \rangle \quad (7)$$

has a uniform charge density everywhere. The act of projecting Eq. (6) for far-separated sites  $i$  and  $j$  is therefore “non-local” in that density is transferred from site  $j$  to site  $i$ . In terms of spin, the state  $| i\sigma, j\sigma' \rangle$  is an eigenstate of  $S_i^z$  and  $S_j^z$  with eigenvalue  $\sigma$  and  $\sigma'$ , respectively. The expectation value of spin at other sites is zero. These are “spinons.”

Making charged excitations without spin simply requires annihilating an electron at the center of each spinon. Anderson’s state with “holons” at sites  $i$  and  $j$  is then

$$| ij \rangle \equiv \mathcal{N}_{ij} c_{i\sigma} c_{j\sigma'} | i\sigma, j\sigma' \rangle, \quad (8)$$

where  $\mathcal{N}_{ij}$  is a normalization factor chosen so that  $\langle ij | i'j' \rangle = \delta_{ii'} \delta_{jj'} + \delta_{ij'} \delta_{ji'}$ . Note that the choice of  $\sigma$  and  $\sigma'$  in Eq. (8) is arbitrary, apart from an overall phase factor. The holons defined by Eq. (8) are unconventional quasiparticles with novel statistics originating from the non-local Gutzwiller projection procedure.

*Scheme 2* – An alternate scheme for constructing spinons and holons begins from Slater determinants with uniform charge density but *non-uniform* spin density.<sup>16</sup> In this approach the average charge density is one particle per site even before projection, and the non-locality occurs in the making of the pre-projected Slater determinant.

Spinons are constructed by considering tight binding models like  $\mathcal{H}_\chi$ , but with additional  $\pi$  fluxes localized at the spinon locations. The resulting Hamiltonian  $\mathcal{H}_d$  is illustrated in fig. 4, and the energy spectrum with and without additional fluxes in fig. 5. Adding the localized fluxes leads to the appearance of midgap states as shown in fig. 5 which are localized around the fluxes. Despite the absence of translational symmetry in  $\mathcal{H}_d$ , the half-filled ground state  $| \chi_d \rangle$  has uniform charge density,<sup>16</sup> because of particle-hole symmetry. (This contrasts with the *non-uniform* charge density in the pre-projected spinon state  $c_{i-\sigma} c_{j\sigma'}^\dagger | \chi \rangle$  in scheme 1.) The spin density is non-uniform due to the singly-occupied midgap state, which is localized near the defective plaquette. As in scheme 1, spinons must be constructed in pairs, since the net flux through a periodic system must be an integer multiple of  $2\pi$ . The spinon pair must be connected by a string of negated  $\chi_{ij}$ ’s to maintain a uniform field around each spinon (see fig. 4). Essentially, the non-uniform charge density in the scheme 1 pre-projected spinon state (which leads to non-locality in the subsequent Gutzwiller projection) has been replaced in scheme 2 by magnetic flux insertion, which has long-range consequences for the tight binding matrix elements.

Adding these localized fluxes is analogous to Laughlin’s procedure<sup>2</sup> for creating quasiparticles in a fractional quantum Hall state, although here only *half* a flux quantum is added. Since Gutzwiller projecting a locally charge-neutral state should not qualitatively change the

long-range correlations of the state, the extra  $\pi$  flux at the defective plaquettes should survive Gutzwiller projection, resulting in localized excitations with “semion” statistics halfway between fermion and boson. Charged holons are created in this scheme by removing a site at the center of the added localized flux.

Despite scheme 2’s intuitive appeal, we will not use it further, since we are interested in off-diagonal matrix elements of the hopping Hamiltonian Eq. (2) between holon states at different positions. In scheme 2, this would require working in a mixed basis of two Slater determinants that are ground states of different pre-projected Hamiltonians. Remarkably, it can be shown for a special value of  $m_0$  that schemes 1 and 2 are essentially equivalent (details are given in the appendix). In this work, all our calculations use scheme 1 (Eqs. 6, 7, and 8).

#### IV. HOLON STATISTICS

The charge motion in a spin liquid is governed by the hopping Hamiltonian Eq. (2). The off-diagonal matrix elements of  $\mathcal{H}$  in the holon variational basis  $|ij\rangle$  contain

FIG. 4. Schematic of defect Hamiltonian  $H_d$  used in scheme 2 (described in the text) for creating spinons and holons. (a) A localized flux is added to a plaquette, identified here by a small open circle. To do this, each link between sites crossed by the Dirac string (dashed line) originating at the added flux is multiplied by  $-1$ . At the other end of the string another localized flux is created (not shown). (b) A site is deleted from the system by cutting all links to it (removing all hopping matrix elements to surrounding sites).

FIG. 5. (a) Density of states resulting from the chiral flux Hamiltonian  $\mathcal{H}_\chi$ , Eq. (4) when  $m_0 = 1$  (solid line). The dotted line spectrum was computed on a 512-site system with periodic boundary conditions and broadened with a width 0.01. (b) Density of states resulting from the same 512-site system but with a pair of  $\pi$  flux defects,  $\mathcal{H}_d$  as illustrated in fig. 4. Fluxes have been placed as shown in the inset. Adding the fluxes leads to the formation of midgap states which split off from the upper and lower band, as shown. See the appendix for further discussion of these midgap states.

information regarding the kinetic energy and statistical phase of holons. In particular, these matrix elements are *not* simply given by the bare  $t_{ij}$ . The effective matrix element for one holon hopping from site  $i$  to site  $j$  in the presence of another holon fixed at site  $k$  is given by

$$T_{kij} = -\langle jk | \mathcal{H}_{\text{hop}} | ik \rangle, \quad (9)$$

where  $i$  and  $j$  are nearest-neighbor sites.

We evaluate Eq. (9) using a method described previously.<sup>12</sup> Briefly, we consider a cluster of  $N_\Gamma$  sites embedded in an infinite system. Correlations within the cluster are computed exactly, while correlations outside the cluster are accounted for only approximately. The thermodynamic limit is taken by considering clusters of various shapes and sizes centered on the sites  $i$ ,  $j$ , and  $k$ , and extrapolating to the infinite cluster limit. In practice, this limit is reached when the cluster size exceeds the correlation length  $\xi_\chi$  in the pre-projected Slater determinant  $|\chi\rangle$ . This method is substantially more efficient than exact projection of Slater determinants on finite toroidal systems (see below).

The effective holon hopping matrix element  $T_{kij}$  contains information about holon statistics.<sup>17</sup> Computation of  $T_{kij}$  allows a direct check of the fractional statistics

invoked in the picture of Zou *et al.*<sup>18</sup> The hopping Hamiltonian Eq. (2) restricted to the holon pair basis Eq. (8) is

$$\mathcal{H}_T = - \sum_{ijk} T_{kij} |kj\rangle \langle ki|. \quad (10)$$

In general, we can separate  $T_{kij}$  into a magnitude and a phase,

$$T_{kij} = |T_{kij}| \exp \left( i \int_i^j \mathbf{A}(k, \mathbf{l}) \cdot d\mathbf{l} \right), \quad (11)$$

where the phase is interpreted as the line integral of an effective vector potential,  $\mathbf{A}$ . This vector potential can be separated<sup>19</sup> into two distinct parts:  $\mathbf{A}(k, \mathbf{l}) = \mathbf{A}_0(\mathbf{l}) + \mathbf{A}_S(k, \mathbf{l})$ . The part of  $\mathbf{A}$  which is independent of the position of site  $k$  is absorbed into  $\mathbf{A}_0$ , and corresponds to a uniform background magnetic flux through which the holons move. The remaining part  $\mathbf{A}_S$  depends on the relative holon position.

Since the holon wavefunctions Eq. (8) can be made symmetric under holon interchange,<sup>20</sup> the vector potential  $\mathbf{A}_S$  contains complete information about the holon statistics. Consider moving one holon around a partner which is held fixed at site  $k$ . The net phase factor for hopping one holon completely around another fixed holon is  $\oint \mathbf{A}_S \cdot d\mathbf{l} \equiv 2\Phi_S$ . When the moving holon path is made infinitely large,  $\Phi_S$  is the statistical phase for holon interchange.<sup>17</sup>

To implement this program, we first compute the background vector potential  $\mathbf{A}_0$  by calculating  $T_{kij}$  when  $k$  (the fixed holon location) is far from  $i$  and  $j$  (the initial and final moving holon locations). We find numerically that the background flux is indistinguishable from the fictitious uniform flux introduced in the pre-projected state. The vector potential  $\mathbf{A}_0$  corresponds to a uniform flux of  $\pi$  through each elementary plaquette, as explicitly included in  $\mathcal{H}_\chi$ . To compute  $\mathbf{A}_S$  we again calculate<sup>21</sup>  $T_{kij}$ 's on a path circling the fixed partner holon, and subtract the contribution from  $\mathbf{A}_0$ .

What is the ‘‘form factor’’ of the statistical flux bound to each holon? One might expect that the bound flux would be distributed in a region of linear extent  $\xi$  about the holon. The statistics would only be well-defined for holons separated by this distance. This situation is similar to the case of the <sup>4</sup>He atom, which is a composite of six fermions that behaves as a boson only on length scales longer than a Bohr radius, so that the internal atomic structure is essentially fixed.

Surprisingly, we find that for the holon wavefunctions Eq.(8) the statistical flux around each holon is sharply peaked in its immediate vicinity, and that the radius of the bound flux tube is the lattice spacing, not the spin correlation length. Figure 6 shows the statistical field density  $\oint_C \mathbf{A}_S \cdot d\mathbf{l}$  where the path  $C$  encloses one plaquette, plotted against the plaquette’s geometrical distance from the origin. Most of the statistical flux is concentrated in the core region immediately surrounding the

FIG. 6. Statistical field density  $\oint_C \mathbf{A}_S \cdot d\mathbf{l}$  through the elementary plaquettes surrounding a fixed holon, when  $m_0 = 1$  (filled circles),  $m_0 = 0.4$  (open squares), and  $m_0 = 0.2$  (open circles). Monte Carlo statistical error bars are approximately the same size as the circles. The inset illustrates the positions of the plaquettes whose field density has been plotted; each data point is accompanied by a letter corresponding to its location.

holon (four plaquettes). Thus the phase shown in fig. 7 represents the total statistical phase for far-separated holons.

Figure 7 shows the statistical flux  $\Phi_S$  threading a small  $2 \times 2$  square loop around a fixed holon as a function of  $m_0$ . For small  $m_0$ , the spin-spin correlation length tends to infinity, and the statistical flux through this small path vanishes. For  $m_0$  of order unity, the spin-spin correlation length is essentially the lattice constant, and the statistical flux nears  $\pi/2$ .

A slight negative contribution may be present outside the core (see fig. 6, especially the filled points representing  $m_0 = 1$ ). We are unable to determine whether this contribution is present for inter-holon separations exceeding  $\sim 5$  lattice constants. Thus we cannot rule out the possibility that a small statistical flux density at large distances from a holon integrates to give a significant contribution to  $\Phi_S$ . The existence of such a long-range tail to the flux distribution could make the holon statistics ill-defined, since the net phase would depend on the inter-holon separation. Neglecting this possible long-range part of the flux distribution, we conclude that the effective statistics of the excitations defined by Eq. (8) are continuously adjustable between values of zero (corresponding to a boson) and  $\pi/2$  (a ‘‘semion’’).

Using an analogy with the fractional quantum Hall effect, Laughlin and Zou have argued<sup>18</sup> that the holon statistics in chiral spin liquids should be *quantized* as semions. Although the logic of this argument seems strong, our calculations (and the numerical calculations of ref. 18) find a statistical phase that is *not* simply  $\pi/2$ . Since here we have carefully considered extrapolation to the thermodynamic limit, this is not the source of the dis-

FIG. 7. Total phase accumulated by hopping one holon around another for the shaded loop shown in the inset, as a function of the mass parameter  $m_0$ . This is the core contribution to twice the statistical phase,  $2\Phi_S$ . The filled circles are computed using the cluster method, after extrapolation to the thermodynamic limit. The open circles represent the same quantity calculated on an  $8 \times 8$  torus, which suffers from a discrete sampling effect and is inaccurate (see text). Monte Carlo statistical error bars are approximately the same size as the circles. The lines are guides to the eye.

crepancy. There are two possible resolutions: (1) there is a weak, longer-range tail to the statistical flux distribution which we cannot resolve in our calculations, but which adds up to enforce  $\Phi_S = \pi/2$ , or (2) the variational states we have considered are *not* good holon states for small  $m_0$ , but only for  $m_0$  of order unity. It is only for such  $m_0$  that the correspondence between scheme 1, scheme 2, and the construction of Laughlin and Zou<sup>18</sup> has been firmly established.

Our embedded cluster results agree with calculations performed on finite tori when properly extrapolated to the thermodynamic limit. While the two methods converge to the same result, the toroidal calculations converge much more slowly, and with important finite size effects. (This is also true for spin-spin correlations.<sup>12</sup>) To confirm this we calculated the core contribution to the statistical phase for  $L \times L$  tori with  $L = 4, 6, 8, 10, 12, 14, \text{ and } 16$ . To confront the worst-case scenario for finite size effects we studied small  $m_0$  in detail, where the correlation length  $\xi$  is longest. Fig. 8 shows the statistical phase from the nearest four plaquettes for  $m_0 = 0.01$  and various toroidal systems. The embedded cluster method rapidly converges to zero statistical flux, as does the sequence of tori with  $L = 4n + 2 = 6, 10, 14, \dots$ . The sequence of tori with  $L = 4n = 4, 8, 12, 16, \dots$  also extrapolate to zero, but surprisingly slowly. This is likely due to the discrete Brillouin zone sampling at special symmetry points for these tori, a flaw which is not present in our

FIG. 8. Extrapolation to the thermodynamic limit  $N \rightarrow \infty$  of the core contribution to the statistical flux (shown in fig. 7) when  $m_0 = 0.01$ . ( $N$  is the number of sites in the projected Slater determinant.) Open squares represent  $4n \times 4n$  toroidal systems, solid squares  $(4n+2) \times (4n+2)$  toroidal systems. The  $4n \times 4n$  toroidal systems suffer from an effect resulting from the discrete sum over the single particle Brillouin zone of  $H_\chi$ , Eq. (4). Open circles indicate the result obtained with  $N$ -site circular clusters embedded in an infinite system. The dashed line shows the result for a small embedded cluster ( $N = 13$ ), at which point convergence has already been reached for the phase information in  $T_{kij}$ . The Monte Carlo statistical error bars are smaller than the markers.

embedded cluster method. This accounts for the apparent discrepancy between the  $8 \times 8$  torus results and the embedded cluster method in fig. 7. (The  $4 \times 4$  torus is a particularly extreme case: the Slater determinant ground state wavefunction of  $H_\chi$  is then *independent* of  $m_0$  due to this sampling effect.) From this calculation we conclude that the finite tori and embedded cluster methods agree when extrapolated to the infinite system limit.

## V. PAIR STATES

We can now compute the pair wavefunction for two holons moving through a chiral spin liquid background by simply numerically diagonalizing  $\mathcal{H}_T$  in the two-holon basis Eq. (8). We find that the lowest-energy two-holon bound state is a complex  $d$ -wave state which breaks T and P symmetries.<sup>22</sup>

To diagonalize  $\mathcal{H}_T$ , we note that this two-body Hamiltonian is invariant under the same set of (magnetic) lattice translations as  $H_\chi$ . Bloch's theorem then states that each pair wavefunction can be labeled by a center of mass momentum  $\mathbf{K}$ , and must have the form

$$|\Phi\rangle_{\mathbf{K}} = \sum_{i < j} e^{i\mathbf{K} \cdot (\mathbf{r}_i + \mathbf{r}_j)/2} \phi(ij)|ij\rangle, \quad (12)$$

where  $\mathbf{r}_i$  is the position of site  $i$ , and the relative wavefunction  $\phi(ij)$  depends only on the lattice translation bringing site  $j$  into the same magnetic unit cell as site  $i$ , as well as the basis indices of the two sites.

TABLE I. Holon interactions. Hopping matrix element  $T$  for one holon fixed at site  $i$  and another moving from site  $j$  to site  $k$  when  $m_0 = 1$ . In the radial case sites  $i$ ,  $j$ , and  $k$  are collinear, in the azimuthal case the hopping direction ( $jk$ ) is perpendicular to ( $ij$ ). In each case  $d_{jk} > d_{ij}$ .

$d_{ij}$	$ T_{ijk} /t$		$V_{ij}/J$
	radial	azimuthal	
1	$0.814 \pm 0.003$	$0.827 \pm 0.004$	$1.20 \pm 0.08$
2	$0.806 \pm 0.002$	$0.804 \pm 0.004$	
3		$0.811 \pm 0.002$	$1.36 \pm 0.1$
5	$0.808 \pm 0.002$	$0.805 \pm 0.003$	$1.45 \pm 0.1$

By diagonalizing  $\mathcal{H}_T$  we find the doubly charged ground state  $|\Phi\rangle$  in our variational basis. This calculation of two holons in a chiral spin liquid resembles in spirit Cooper's original demonstration that a pairing instability exists for two electrons attracting above a Fermi sea. The effective holon hopping Hamiltonian  $\mathcal{H}_T$  provides a kinetic resonance energy of order a few percent  $t$  for nearby holons, because the magnitude  $|T_{ijk}|$  is enhanced when sites  $i$  and  $j$  (or  $i$  and  $k$ ) are close (see table I). Also, we have up until now neglected a static interaction  $V_{ij}$  between holons at sites  $i$  and  $j$  which arises from the spin interaction, Eq. (1):

$$V_{ij} = J \sum_{\langle lm \rangle} (\langle ij | \mathbf{S}_l \cdot \mathbf{S}_m | ij \rangle - \langle \chi | P_G \mathbf{S}_l \cdot \mathbf{S}_m P_G | \chi \rangle). \quad (13)$$

Roughly speaking,  $V_{ij}$  provides a short-range static attraction because neighboring holons can share a broken antiferromagnetic bond. In the undoped spin liquid, each unbroken bond contributes an energy  $J\langle \mathbf{S} \cdot \mathbf{S} \rangle_{\text{NN}} = (-0.205 \pm 0.005)J$  when  $m_0 = 1$ . To estimate the static holon potential we compute  $\langle ij | \mathbf{S}_l \cdot \mathbf{S}_m | ij \rangle$  for the nearest-neighbor sites ( $lm$ ) around a holon pair fixed at sites  $i$  and  $j$  using the embedded cluster method. Table I summarizes the results when  $m_0 = 1$ . A far-separated holon pair (5 lattice constants apart) breaks eight antiferromagnetic bonds, costing  $8 \times |J\langle \mathbf{S} \cdot \mathbf{S} \rangle_{\text{NN}}| \sim 1.6J$ , but the remaining nearby bonds are strengthened, so isolated holons end up costing slightly less energy to create. As the holons are brought closer together, they eventually share a broken bond, causing a net attractive potential of strength  $\sim 0.3J$ . Since both the kinetic resonance and the static potential are attractive, the variational ground state  $|\Phi\rangle_{\mathbf{K}}$  is a bound state of two holons. Numerically, we find that the lowest energy bound state has center of mass momentum  $\mathbf{K} = 0$ , and effective mass  $m^* \equiv 1/(\partial^2 E/\partial K^2) \sim 3m$ , where  $m = 4|T|$  is the effective mass of an isolated holon with hopping matrix element  $T$ , evaluated for far-separated holons.

What is the symmetry of the pair state  $|\Phi\rangle$ ? To answer this question, consider the relative pair wavefunction  $\phi(ij)$ . Since the relative phases of the holon pair states  $|ij\rangle$  for different  $ij$  depend on the arbitrary choice of gauge used to construct the Slater determinant  $|\chi\rangle$ , the relative phase of  $\phi(ij)$  are also gauge dependent. This

FIG. 9. Overlap between  $|(ij)\rangle$  (a singlet hole pair, Eq.(14)) and  $|ij\rangle$ , (a holon pair, Eq.(8)) as a function of geometrical distance  $d_{ij}$  between sites  $i$  and  $j$  when (a)  $m_0 = 1$ , (b)  $m_0 = 0.4$ , (c)  $m_0 = 0.2$ . For a given pair, site  $j$  may lie on the same sublattice (open circles) or the opposite sublattice (filled circles) as site  $i$ . The correlation length  $\xi_\chi$  is indicated in each frame. The dominant overlap occurs for nearest-neighbor pairs, and is close to unity over the entire range of  $m_0$ . The overlaps are large for pairs closer than  $\xi_\chi$ , and are slightly larger for opposite sublattice pairs than for same sublattice pairs. The Monte Carlo statistical error bars are approximately the same size as the circles.

complication can be eliminated by projecting the two-holon state  $|\Phi\rangle$  into the set of states comprising a singlet hole pair added to the undoped spin liquid:

$$|(ij)\rangle = \mathcal{M}_{ij} (c_{i\uparrow}c_{j\downarrow} - c_{i\downarrow}c_{j\uparrow}) P_G |\chi\rangle. \quad (14)$$

Here  $\mathcal{M}_{ij}$  is a normalization factor chosen so that  $\langle (ij) | (i'j') \rangle = \delta_{ii'}\delta_{jj'} + \delta_{ij'}\delta_{ji'}$ . These hole pair states are independent of the gauge choice in  $|\chi\rangle$ , since  $P_G |\chi\rangle$  has precisely one particle per site, and is independent of gauge choice. The inner product

$$\Phi(ij) = \langle (ij) | \Phi \rangle \quad (15)$$



FIG. 10. The relative pair wavefunction  $\Phi(i, j)$ . all  $\phi_n$  are real numbers. The symmetry is a combination of  $d_{x^2-y^2}$  and  $d_{xy}$ .

is then a gauge invariant description of that part of the two-holon state which resembles a singlet hole pair.

How similar are two holons and a singlet hole pair? The overlap between these two states is simply an expectation value in the state  $|\chi\rangle$

$$\langle (ij)|ij\rangle = 2\mathcal{N}_{ij}\mathcal{M}_{ij}\langle\chi|P_G(1 - n_{i\uparrow})n_{j\uparrow}c_{i\downarrow}^\dagger c_{j\downarrow}|\chi\rangle, \quad (16)$$

and can be computed using the embedded cluster method: The magnitude of this overlap versus inter-holon distance  $d_{ij}$  is plotted in fig. 9 for three different values of  $m_0$ . A nearest-neighbor holon pair is essentially identical to a singlet hole pair, as shown by the near-unit overlap in fig. 9 at  $d_{ij} = 1$  in all three cases. The overlap decays quickly as sites  $i$  and  $j$  are separated, presumably since far-separated holons disrupt the system differently than holes. Holes maintain a strong spacial correlation between spin and charge, while the holon has no spin. When holons are close together, however, the composite object has charge  $2e$  and spin-0, permitting an overlap with a singlet hole pair with the same quantum numbers. The decay of the overlap with distance occurs on a length scale roughly equal to the correlation length  $\xi_\chi$ , as shown in fig. 9.

Using Eq. (16) and the two-holon state  $|\Phi\rangle$  obtained by exact diagonalization of  $\mathcal{H}_T$ , we can compute the “hole pair wavefunction” (the inner product Eq. (15)) for inter-holon separations up to 4 lattice constants. Figure 11 shows the radial probability density  $|\Phi(ij)|^2$  as a function of the inter-holon distance  $d_{ij}$ . The amplitude is mostly concentrated near the origin, due to the kinetic resonance effect already mentioned and the short range of the holon pair/hole pair overlap. Further static local attraction due to the sharing of broken bonds only enhances this effect,

FIG. 11. Probability density in the two-holon wavefunction  $\Phi(ij)$  versus inter-holon separation for holons governed by  $\mathcal{H}_T$  with  $m_0 = 1$  (filled circles),  $m_0 = 0.2$  (open circles). In each case the wavefunction’s angular symmetry is  $d$ -wave as illustrated in fig. 10.

without changing the angular symmetry of the state, as we verified numerically by considering additional short-range static attraction mimicking  $V_{ij}$ .

For all values of  $m_0$ , the relative hole pair wavefunction  $\Phi(ij)$  has  $d$ -wave symmetry (i.e., the state changes sign under 90 degree rotation), as illustrated in fig. 10. Because of the explicit breaking of time-reversal and parity in the chiral spin liquid, this state is a complex linear combination of  $d_{x^2-y^2}$  and  $d_{xy}$  states. (Although these states transform as different irreducible representations of the tetragonal group, they are mixed in the group of four-fold rotations that remains when reflections are removed from the tetragonal group.<sup>22</sup>) As shown in fig. 10, the relative pair wavefunction is purely real on the  $x$  and  $y$  axes, and purely imaginary along the diagonals;  $\Phi(ij)$  is permitted by symmetry to be a general complex number elsewhere, but we find that it remains either purely real or imaginary in non-symmetry directions as well.

Since the two-holon state  $|\Phi\rangle$  has substantial overlap with a two-hole state, it is natural to consider a multi-holon state obtained by macroscopically occupying the hole pair wavefunction  $\Phi(ij)$ , thus arriving at a BCS superconductor with a  $d$ -wave Cooper wavefunction. To show that this is the ground state of  $\mathcal{H}$  or a similar spin Hamiltonian requires a much more elaborate calculation than we have given here. Nevertheless, if we assume that the “anyon condensate” of Laughlin *et al.* is obtained by a Bose condensation of holon pairs, then we may infer from our calculation that such a state will have *conventional* electron-pair off-diagonal long-range order:

$$\lim_{|(ij)-(i'j')|\rightarrow\infty} \langle c_{i\uparrow}^\dagger c_{j\downarrow}^\dagger c_{i'\downarrow} c_{j'\uparrow} \rangle \rightarrow \Psi^*(ij)\Psi(i'j'). \quad (17)$$

The order parameter  $\Psi(ij)$  is nothing more than the internal Cooper pair wavefunction, which for dilute, non-overlapping pairs should be given simply by the relative

hole-pair wavefunction  $\Phi(ij)$  we have calculated above. Thus a holon condensate is expected to possess all of the features of a BCS superconductor that has the unconventional  $d$ -wave order parameter described above. Most strikingly, such a  $d$ -wave state is expected to have a full energy gap, since there are no nodes in the Cooper pair wavefunction.

## VI. CONCLUSIONS

We have investigated the properties of charged excitations in a chiral spin liquid on a square lattice, using a variational basis which explicitly separates the spin and charge degrees of freedom. By directly computing the off-diagonal Hamiltonian matrix elements of the holon excitations, we found that the statistics of the excitations described by these variational states vary *continuously* between boson ( $\Phi_S = 0$ ) and semion ( $\Phi_S = \pi/2$ ). The gauge field responsible for the statistical phase is localized in the area surrounding the holon, with a core size comparable to the lattice spacing.

These results may be intuitively understood by viewing holons and spinons as topological excitations in a chiral tight-binding model.<sup>16</sup> In the appendix we show that this picture (while computationally more difficult to implement) is an essentially equivalent representation of Andersons holons for spin liquids with short spin-spin correlation lengths.

The two-holon ground state has total momentum zero, and its relative wavefunction transforms as a linear combination of the  $d_{x^2-y^2}$  and  $d_{xy}$  representations of the tetragonal group. Such a linear combination is permitted<sup>22</sup> by the explicit breaking of T and P symmetry in the chiral spin liquid. Two factors contribute to the formation of a two-holon bound state: (a) a static attraction of order  $J$  between holons, and (b) a kinetic resonance due to enhanced holon hopping in the vicinity of another holon.<sup>23</sup> These effects are reminiscent of a “spin bag,” in that the local environment around one holon lowers the energy of a second in its vicinity.

The pair wavefunction of a bound holon pair has significant overlap with a bound singlet hole pair, especially at short distances. This overlap suggests that a holon pair condensate is closely related to a hole pair (or electron) condensate, as found in the BCS theory of superconductivity. We conclude that a superconductor arising from a pair condensate of bound holons is a BCS-like superconductor with a gap function with  $d$ -wave symmetry.<sup>22</sup> Such a superconductor would be fully gapped, since by mixing to  $id_{xy}$  the gap function avoids crossing zero. This superconductor can be described *either* as a  $d$ -wave BCS superconductor or as an anyonic superconductor. These two languages are evidently equivalent ways to describe the same state.

## ACKNOWLEDGMENTS

We thank K.G. Singh for useful discussions, and P.E. Lammert for useful discussions and a careful reading of the manuscript. Work at Berkeley was supported by the NSF under grant DMR-91-57414 and by the US Dept. of Education. D.S.R. acknowledges a grant from the Alfred P. Sloan Foundation.

## APPENDIX: EQUIVALENCE OF HOLON SCHEMES

In this appendix we show that the Anderson-holon and the topological charged excitations described previously in ref. 16 are equivalent. This equivalence provides an intuitive picture of the Anderson-holon excitation and some insight into its local structure. The argument relies heavily on the equivalence between an Anderson-holon wavefunction and the Kalmeyer-Laughlin wavefunction established by Laughlin and Zou<sup>18</sup> so we start by briefly recalling the content of their proof.

In ref. 18 it is shown that the state obtained by Gutzwiller projecting the ground state of  $H_\chi$  at half-filling and with  $m_0 = 2e^{-\pi/4} \approx 0.912$  is identical to the Kalmeyer-Laughlin (KL) state.<sup>24</sup> In first quantization, the KL state is expressed by the wavefunction

$$\psi_{KL}(z_1, \dots, z_{N/2}) = \prod_{\mu < \nu}^{N/2} (z_\mu - z_\nu)^2 \prod_{\gamma=1}^{N/2} G(z_\gamma) \exp \left[ -\frac{|z_\gamma|^2}{4} \right], \quad (\text{A1})$$

where  $z_\gamma = (m_\gamma + in_\gamma)$  is a complex number defining the position of an up spin labeled by  $\gamma$  at square lattice coordinates  $(m, n)$ , and  $G(z)$  is a gauge-dependent function.  $G(z) = (-1)^{(n+m+nm)}$  in the gauge chosen by the authors of ref. 18.

The proof consists of two steps. In the first it is shown that given the first-quantized version of the *up spin* part of the half-filled ground state of  $H_\chi$  – a function  $\phi(\{\mathbf{r}\})$  where the set of coordinates  $\{\mathbf{r}\} \equiv \mathbf{r}_1, \dots, \mathbf{r}_{N/2}$  describes the position of  $N/2$  up electrons on a lattice of  $N$  sites – one can write down the wavefunction corresponding to the Gutzwiller projected state  $\Psi$  as a function of the same set of coordinates:

$$\Psi(\{\mathbf{r}\}) = \phi^2(\{\mathbf{r}\}) e^{if(\{\mathbf{r}\})}, \quad (\text{A2})$$

where the function  $f(\{\mathbf{r}\})$  depends on the choice of the basis used to represent  $\Psi$ . (See Eq. (A12) for a precise definition.) In the second step it is shown that with a particular choice<sup>24</sup> of  $m_0$ , the Slater determinant obtained by filling the lower band of  $H_\chi$  coincides with the determinant obtained by filling the energy levels corresponding to an electron in free space moving in a uniform magnetic field with  $l = (\hbar c/eB)^{1/2} = 1/\sqrt{\pi}$ , provided the single-particle wavefunctions defined on a continuum are

restricted to points on a square lattice with lattice constant equal to unity. This representation of  $\phi$ , together with Eq. (A2) is then used to show that  $\Psi = \psi_{KL}$ . As a simple corollary, Zou and Laughlin show that the wavefunction corresponding to an Anderson-holon pair at sites  $A$  and  $B$  is represented by

$$|z_A, z_B\rangle = \prod_{\gamma} (z_{\gamma} - z_A)(z_{\gamma} - z_B) \prod_{\mu < \nu} (z_{\mu} - z_{\nu})^2 \times \prod_{\gamma} G(z_{\gamma}) \exp\left[-\frac{|z_{\gamma}|^2}{4}\right]. \quad (\text{A3})$$

Our approach is very similar. First we show that the first step follows generally when a particle-hole symmetry operator exists, thus it also applies to the class of Hamiltonians  $H_d$  described in ref. 16. Second, we argue that a representation of the filled lower band of  $H_d$  is obtained by filling the first Landau level corresponding to an electron in a uniform field with two flux tubes of appropriate strength at position  $\mathbf{r}_A$  and  $\mathbf{r}_B$ , again having restricted the wavefunction to points on a square lattice. Although we will not prove this point rigorously it is a natural assumption in view of the results of ref. 18.

The Hamiltonian  $H_d$  describing the topological charged excitation of section II's scheme 2 is obtained from  $H_{\chi}$  by adding flux defects in the form of an additional half-flux quantum  $\pi$  through a plaquette adjacent to site  $A$ , the same through a plaquette adjacent to site  $B$ , and a string of  $\pi$  phase additions to the phases of the  $\chi_{ij}$ 's between sites  $A$  and  $B$  to restore the proper flux in the remaining plaquettes.<sup>16</sup> (The actual position of this string is irrelevant, as it can be moved by a suitable gauge transformation.) Note that the added fictitious flux couples only to the particles' orbital motion.

It is convenient to start with  $H_{\chi}$  (and  $H_d$ ) expressed in a gauge such that the  $\chi_{ij}$  are real for nearest-neighbor and imaginary for next-nearest neighbor bonds. This choice of phases for the link variables allows a simple definition of the particle-hole conjugation operator  $\Upsilon$ , which we define to be the *linear* operator satisfying

$$\begin{aligned} \Upsilon|\text{vac}_{\sigma}\rangle &= e^{i\alpha}|F_{\sigma}\rangle, \\ \Upsilon^{-1}c_{\mathbf{r}\sigma}\Upsilon &= e^{i\mathbf{r}\cdot\mathbf{Q}}c_{\mathbf{r}\sigma}^{\dagger}, \end{aligned} \quad (\text{A4})$$

where  $\alpha$  is an arbitrary phase,  $\mathbf{Q} \equiv (\pi, \pi)$ ,  $|\text{vac}_{\sigma}\rangle$  is the vacuum state in the  $\sigma$  spin subspace, and  $|F_{\sigma}\rangle = \prod_{\{\mathbf{r}\}} c_{\mathbf{r}}^{\dagger}|\text{vac}_{\sigma}\rangle$  is the state with one  $\sigma$  electron at each of the  $N$  sites in the system. To avoid ordering ambiguities this product is performed in an (arbitrary) order specified by an ordering function  $O(\mathbf{r})$  numbering the sites of the lattice from 0 to  $N-1$  such that  $O(\mathbf{r}_1) < O(\mathbf{r}_2) < \dots < O(\mathbf{r}_N)$ .

With this definition of  $\Upsilon$  one can show that  $\Upsilon$  is unitary and  $\Upsilon^2 = e^{i\gamma}$ , where  $\gamma$  depends only on  $N$  and  $\alpha$ . The usefulness of  $\Upsilon$  is apparent when we realize that  $\Upsilon$  is a symmetry operation for both  $\mathcal{H}_{\chi}$  and  $\mathcal{H}_d$ :  $[\Upsilon, H_{\chi}] = [\Upsilon, H_d] = 0$ . Notice that both charge density

and current density are odd under particle-hole symmetry, that is  $\Upsilon^{\dagger}(1 - n_{\mathbf{r}})\Upsilon = n_{\mathbf{r}} - 1$ ,  $\Upsilon^{\dagger}J_{\mathbf{a}}\Upsilon = -J_{\mathbf{a}}$ , where  $J_{\mathbf{a}} = i \sum_{\sigma} (e^{i\phi_{\mathbf{a}}} c_{\mathbf{r},\sigma}^{\dagger} c_{\mathbf{r}+\mathbf{a},\sigma} - \text{H.c.})$ .

We also define the *antilinear* operator  $Q$  :

$$\begin{aligned} Q|\text{vac}_{\sigma}\rangle &= |F_{\sigma}\rangle, \\ Q^{-1}c_{\mathbf{r}\sigma}Q &= c_{\mathbf{r}\sigma}^{\dagger}. \end{aligned} \quad (\text{A5})$$

$Q$  is antiunitary, anticommutes with  $H_{\chi}$  and  $H_d$ , and commutes with  $\Upsilon$ . A simple consequence of the commutation relations of  $Q$ ,  $\Upsilon$ , and the Hamiltonians  $H_d$  or  $H_{\chi}$  is that single-particle states always come in pairs,  $|E_{\sigma}\rangle$  and  $Q\Upsilon|E_{\sigma}\rangle$ , corresponding to energies  $E$  and  $-E$  respectively. Since in the absence of flux tubes and at half filling the ground state of  $H_{\chi}$  is fully gapped, symmetry suggests (and calculations have explicitly shown<sup>16</sup>) that with a single flux-tube and an odd number of sites the energy spectrum of  $H_d$  will have a midgap state, whose amplitude is localized near the flux tube. With an even number of sites and two flux-tubes at  $\mathbf{r}_A$  and  $\mathbf{r}_B$  the degeneracy of the two midgap states in the energy spectrum of  $H_d$  is lifted by  $\Delta E_{\text{loc}}$ , which is exponentially small in  $|\mathbf{r}_A - \mathbf{r}_B|$ . (See fig. 5.)

Our task now is to evaluate the Gutzwiller-projected two-holon wavefunction of ref. 16. This is obtained by first considering the ground state at half-filling  $|\chi_d\rangle$  of  $H_d$  when fluxes have been added at sites  $A$  and  $B$ , and these same sites have been removed from the lattice. Notice that the removal of the two sites eliminates the two midgap states and that the ground state is non-degenerate and hence invariant under  $\Upsilon$ .

After Gutzwiller projection every configuration has a single electron at each site and an equal number of up and down electrons. A convenient basis in which to represent  $P_G|\chi_d\rangle$  is

$$|\{\mathbf{r}\}\rangle = S_{\tilde{\mathbf{r}}_1}^{-} \cdots S_{\tilde{\mathbf{r}}_M}^{-} |F_{\uparrow}\rangle, \quad (\text{A6})$$

where  $S_{\tilde{\mathbf{r}}}^{-} = c_{\tilde{\mathbf{r}}\downarrow}^{\dagger} c_{\tilde{\mathbf{r}}\uparrow}$  is the usual spin lowering operator,  $\{\mathbf{r}\}$  denotes the set of positions of the up spin electrons, and  $\{\tilde{\mathbf{r}}\}$  denotes the set complementary to  $\{\mathbf{r}\}$  specifying the positions of the down spin electrons. The sets  $\{\mathbf{r}\}$  and  $\{\tilde{\mathbf{r}}\}$  each contain  $M = N/2 - 1$  members.

The Gutzwiller-projected wavefunction in this basis is given by

$$\Psi(\{\mathbf{r}\}) \equiv \langle \{\mathbf{r}\} | P_G |\chi_d\rangle = \langle \{\mathbf{r}\} | \chi_d\rangle, \quad (\text{A7})$$

since none of the states  $|\{\mathbf{r}\}\rangle$  contain site double-occupancy. Using the anticommutation properties of fermion operators, we find

$$\langle \{\mathbf{r}\} | \chi_d\rangle = \exp\left[i\pi \sum_{i=1}^M O(\tilde{\mathbf{r}}_i)\right] \phi_d(\{\mathbf{r}\}) \phi_d(\{\tilde{\mathbf{r}}\}), \quad (\text{A8})$$

where

$$\phi_d(\{\mathbf{r}\}) \equiv \langle \text{vac}_{\uparrow} | c_{\mathbf{r}_M} \cdots c_{\mathbf{r}_1} | \chi_d \rangle, \quad (\text{A9})$$

and we have made the decomposition  $|\chi_d\rangle = |\chi_{d\uparrow}\rangle \otimes |\chi_{d\downarrow}\rangle$  and dropped the explicit spin indices on  $c_{\mathbf{r}}$  and  $c_{\mathbf{r}}^\dagger$ . We can now use the properties of  $\Upsilon$  to obtain

$$\begin{aligned} \phi_d(\{\tilde{\mathbf{r}}\}) &= \langle \text{vac}_\uparrow | c_{\tilde{\mathbf{r}}_M} \cdots c_{\tilde{\mathbf{r}}_1} | \chi_{d\uparrow} \rangle \\ &= \langle \text{vac}_\uparrow | \Upsilon \Upsilon^\dagger c_{\tilde{\mathbf{r}}_M} \Upsilon \cdots \Upsilon^\dagger c_{\tilde{\mathbf{r}}_1} \Upsilon \Upsilon^\dagger | \chi_{d\uparrow} \rangle \\ &= \exp \left[ i \sum_{i=1}^M \mathbf{Q} \cdot \tilde{\mathbf{r}}_i \right] \langle F_\uparrow | c_{\tilde{\mathbf{r}}_M}^\dagger \cdots c_{\tilde{\mathbf{r}}_1}^\dagger | \chi_{d\uparrow} \rangle \\ &= \exp \left[ i \sum_{i=1}^M \mathbf{Q} \cdot \tilde{\mathbf{r}}_i + \pi O(\tilde{\mathbf{r}}_i) \right] \langle \text{vac}_\uparrow | c_{\mathbf{r}_M} \cdots c_{\mathbf{r}_1} | \chi_{d\uparrow} \rangle, \end{aligned} \quad (\text{A10})$$

which, together with Eq. (A8), gives

$$\Psi(\{\mathbf{r}\}) = \exp \left[ -i \sum_{i=1}^M \mathbf{Q} \cdot \mathbf{r}_i \right] \phi_d^2(\{\mathbf{r}\}). \quad (\text{A11})$$

In Eq. (A11) we have used the freedom in the choice of  $\alpha$  in Eq. (A4) to eliminate an additional phase independent of  $\{\mathbf{r}\}$ .

Eq. (A11) gives the wavefunction  $\Psi$  in the particular gauge in which the link variables  $\chi_{ij}$  are either real or purely imaginary. Under any local gauge transformation  $c_{\mathbf{r}\sigma} \rightarrow \exp[-i\Lambda(\mathbf{r})] c_{\mathbf{r}\sigma}$  we finally derive, with the help of Eq. (A9),

$$\Psi(\{\mathbf{r}\}) = \exp \left[ -i \sum_1^M \mathbf{Q} \cdot \mathbf{r}_i + 2\Lambda(\mathbf{r}_i) \right] \phi_d^2(\{\mathbf{r}\}; \Lambda), \quad (\text{A12})$$

where we have added explicit dependence on  $\Lambda$  to  $\phi_d$  in order to remind the reader that the up spin part of the ground state  $|\chi_{d\uparrow}\rangle$  is gauge dependent. Eq. (A12) now corresponds directly to Eq. (A2), as desired.

Next, we want to find an alternate representation of  $\phi_d$  based on a continuum picture of electrons moving in a uniform magnetic field with two flux tubes at positions  $A$  and  $B$ . Notice that although by its definition Eq. (A7)  $\Psi$  is gauge invariant,  $\phi_d$  is not, and we must be careful to choose a gauge in the continuum which corresponds to the particular gauge used to derive Eq. (A11) and Eq. (A12). In the following we work in the symmetric gauge although the gauge used to derive Eq. (A11) and used in ref. 18 to express  $|z_A, z_B\rangle$  is the Landau gauge. (Strictly speaking, this gauge differs from the Landau gauge by a ‘singular’ transformation, which will be discussed later.)

We start with the continuum Hamiltonian

$$H = \frac{\hbar^2}{2ml^2} (-i\nabla + \mathbf{A})^2 \quad (\text{A13})$$

where  $\mathbf{A} = (\mathbf{r} \times \hat{\mathbf{z}})/2 + \mathbf{A}_{\mathbf{r}_A} + \mathbf{A}_{\mathbf{r}_B}$ , the unit of length  $l = (\hbar c/eB)^{1/2}$ , and  $B$  has been chosen so that in the absence of flux tubes the degeneracy of the Landau levels is equal to  $N/2$ ; this implies  $B = \phi_0/2$  where  $\phi_0 = hc/e$  is the flux quantum. The vector potential corresponding to a flux tube of strength  $\alpha\phi_0$  is then given by

$$\mathbf{A}_{\mathbf{r}_A}^\theta = \alpha \frac{\theta_A}{|\mathbf{r} - \mathbf{r}_A|} \quad (\text{A14})$$

where  $\theta_A$  is the azimuthal angle measured with respect to  $\mathbf{r}_A$ , and positive values of  $\alpha$  correspond to a localized flux which strengthens the background magnetic field.

It is convenient to gauge away  $\mathbf{A}_{\mathbf{r}_A}$  and  $\mathbf{A}_{\mathbf{r}_B}$  by looking for a solution in the form  $\psi = \tilde{\psi} \exp[-i \int (\mathbf{A}_{\mathbf{r}_A} + \mathbf{A}_{\mathbf{r}_B}) \cdot d\mathbf{l}]$ . Then  $\tilde{\psi}$  obeys the Schrödinger equation for a particle in an uniform field but must be multivalued in order to make  $\psi$  single-valued: when encircling  $\mathbf{r}_A$  and  $\mathbf{r}_B$  the phase of  $\tilde{\psi}$  must change by  $\alpha_A$  and  $\alpha_B$  respectively, in order to compensate for the phase change due to the exponential term in Eq. (A15). But the most general solution corresponding to the lowest Landau level orbitals in the symmetric gauge can be written as  $\tilde{\psi}(z) = \tilde{g}(z) e^{z\bar{z}/8}$ , where  $z = x + iy$  and  $\tilde{g}(z)$  is an arbitrary function of  $z$ . The solution of interest is then given by  $\tilde{g}(z) = (z - z_A)^{\alpha_A} (z - z_B)^{\alpha_B} g(z)$ , with  $g(z)$  analytic everywhere.

Although the solution so defined is valid for any<sup>25</sup> value of  $\alpha_A$  and  $\alpha_B$ , our purposes lead us to consider the special case  $\alpha_A = -\alpha_B = \alpha > 0$ . In this case, as  $\alpha$  is increased from zero, a lone state splits off from each of the  $n = 0$  and  $n = 1$  Landau level manifolds: the first lone state’s energy increases, and the second lone state’s energy decreases. Note that the degenerate Landau level manifolds can be associated with the lower ( $n = 0$ ) and upper ( $n = 1$ ) band of the lattice Hamiltonian  $H_d$ . The two lone states which split off are similarly associated with the two localized states of  $H_d$  in the vicinity of the flux defects. Filling the  $n = 0$  Landau level corresponds to computing the Slater determinant obtained by filling the levels

$$\tilde{\psi}_k(z) = (z - z_A)^\alpha (z - z_B)^{1-\alpha} z^k e^{z\bar{z}/8} \quad (\text{A15})$$

where  $k = 0, 1, \dots$ . The resulting Vandermonde determinant can be easily calculated giving the result

$$\begin{aligned} \phi(z_1, \dots, z_M) &= \prod_\gamma (z_\gamma - z_A)^\alpha (z_\gamma - z_B)^{1-\alpha} \prod_{\mu < \nu} (z_\mu - z_\nu) \\ &\quad \times \prod_\gamma G(z_\gamma) \exp \left[ -\frac{|z_\gamma|^2}{8} \right]. \end{aligned} \quad (\text{A16})$$

To complete the argument we now employ the gauge freedom associated with  $\Lambda$  in Eq. (A12). First notice that the use of  $\tilde{\psi}$  in place of  $\psi$  to obtain Eq. (A16) is justified because the gauge we were effectively using in writing a lattice Hamiltonian with a string of defects connecting sites  $A$  and  $B$  is precisely the singular gauge (singular only in the continuum limit, of course) we employed to go from  $\psi$  to  $\tilde{\psi}$ . Alternatively we could have used  $\psi$  to define  $\phi$  in Eq. (A16) and performed a gauge transformation on the lattice Hamiltonian to smooth out the string connecting  $A$  and  $B$ . When this gauge transformation is properly taken into account as prescribed by Eq. (A12) the result for  $\Psi$  is identical. Finally we have to convert the Landau gauge, corresponding to Eq. (A11), into the

symmetric gauge used to express  $\phi$  in Eq. (A16). This is easily accomplished through the gauge transformation defined by  $\Lambda(\mathbf{r}) = \pi xy/2$  which, when restricted to the lattice  $\mathbf{r} = (m, n)$ , makes the prefactor in Eq. (A12) equal to

$$\exp \left[ -i \sum_1^M \mathbf{Q} \cdot \mathbf{r}_i + 2\Lambda(\mathbf{r}_i) \right] = \prod_{\gamma} (-1)^{m_{\gamma} + n_{\gamma} + m_{\gamma} n_{\gamma}}. \quad (\text{A17})$$

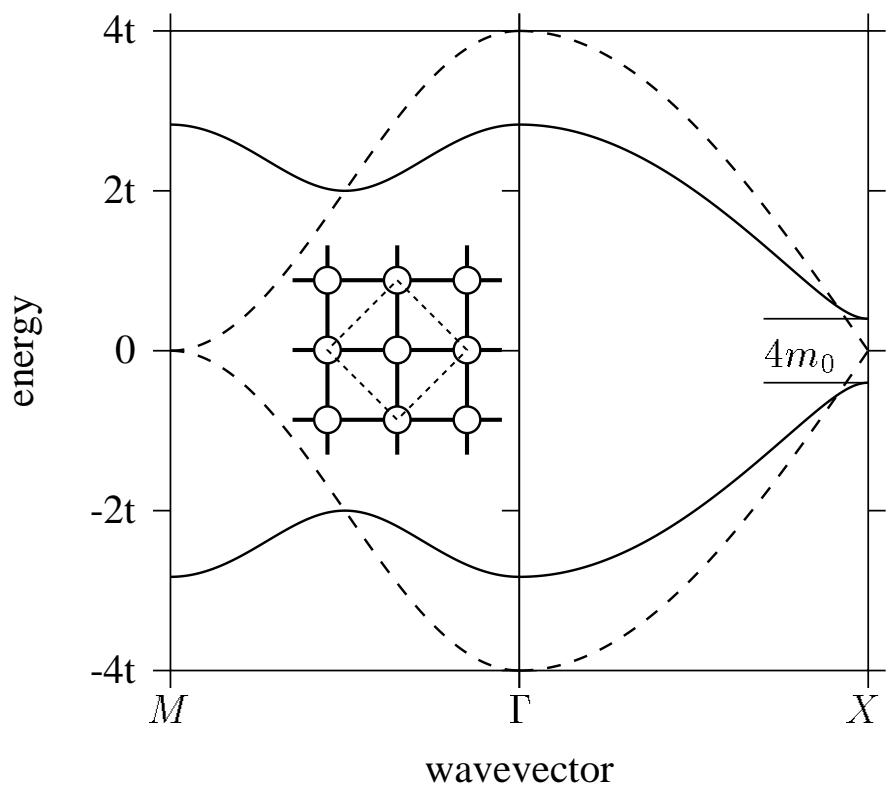
This is identical to the factor  $\prod_{\gamma} G(z_{\gamma})$  appearing in Eq. (A3).

By using Eq. (A12) and Eq. (A16) with the continuum variables  $z_{\gamma}$  restricted to lattice points and  $\alpha = 1/2$ , the equivalence between the two-holon state defined as in Section II, scheme 2, and the Anderson holon state, scheme 1, defined by Eq. (A3) is now explicitly shown.

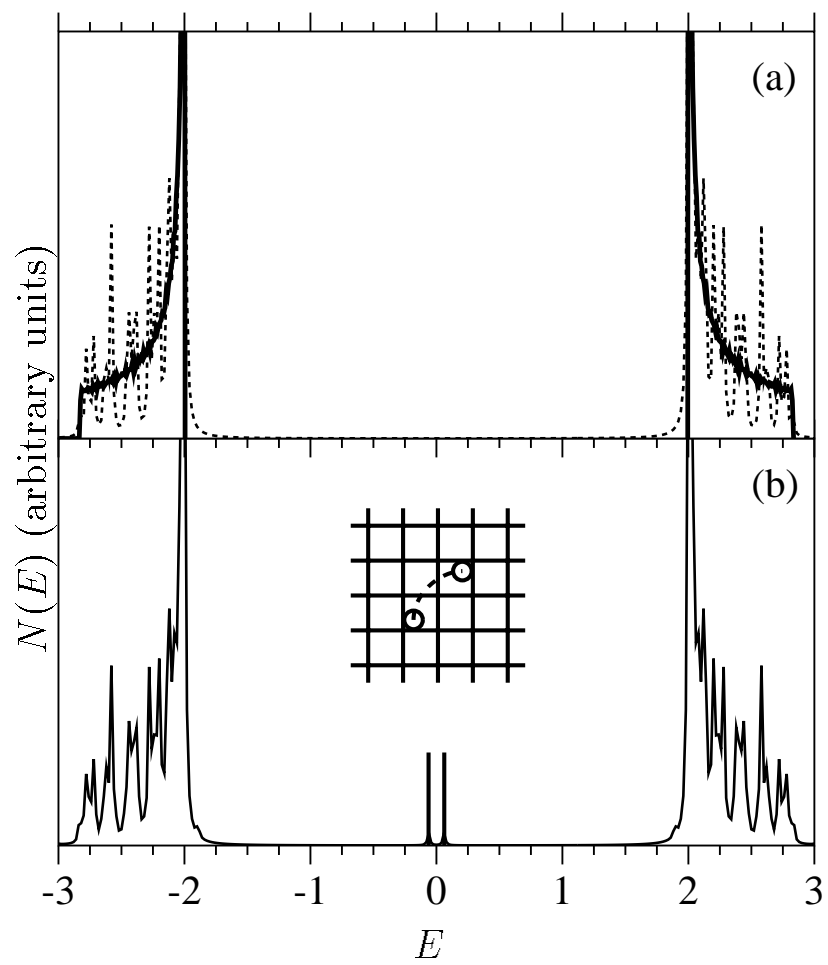
---

<sup>1</sup> L.D. Landau, Sov. Phys. JETP **3**, 920 (1956).  
<sup>2</sup> R.B. Laughlin, in *Two-Dimensional Strongly Correlated Electronic Systems*, ed. Zi-Zhao Gan, Zhao-Bin Su (Gordon and Breach, London; 1989).  
<sup>3</sup> W.P. Su, J.R. Schrieffer and A.J. Heeger, Phys. Rev. B **22**, 2099 (1980).  
<sup>4</sup> P.W. Anderson, Science **235**, 1196 (1987).  
<sup>5</sup> S.A. Kivelson, D.S. Rokhsar, and J.P. Sethna, Phys. Rev. B **35**, 8865 (1987).  
<sup>6</sup> V. Kalmeyer and R.B. Laughlin, Phys. Rev. Lett. **59**, 2095 (1987).  
<sup>7</sup> M. Inui, S. Doniach, and M. Gabay, Phys. Rev. B **38**, 6631 (1988).  
<sup>8</sup> X.-G. Wen, F. Wilczek and A. Zee, Phys. Rev. B **39**, 11413 (1989).  
<sup>9</sup> In a Slater determinant state, same-spin particles avoid one another due to the Pauli principle. The Gutzwiller projector Eq. (3) further limits the state so that *unlike*-spin particles avoid one another. The projected state is then a superposition of configurations of up fermions which do not coincide with the positions of the down fermions. If by construction the spin and charge correlations of the Slater determinant are short-range, for a given down spin configuration a typical up configuration of the Slater determinant needs only local rearrangements to obtain a configuration which survives Gutzwiller projection.  
<sup>10</sup> M.C. Gutzwiller, Phys. Rev. **134**, A923 (1964); M.C. Gutzwiller, Phys. Rev. **137**, A1726 (1965).  
<sup>11</sup> T.C. Hsu, Phys. Rev. B **41**, 11379 (1990); A. Barbieri, A. P. Young, J. Phys. C **3**, 1801 (1991).  
<sup>12</sup> A. Barbieri, D.M. Deaven, and D.S. Rokhsar, Phys. Rev. B **45**, 8288 (1992).  
<sup>13</sup> J.B. Marston and I. Affleck, Phys. Rev. B **39**, 11538 (1989).  
<sup>14</sup> E. Dagotto, Int. J. Mod. Phys. B **5**, 907 (1991); J.D. Reger, J.A. Riera and A.P. Young, J. Phys. Condensed Matter **1**, 1855 (1989).

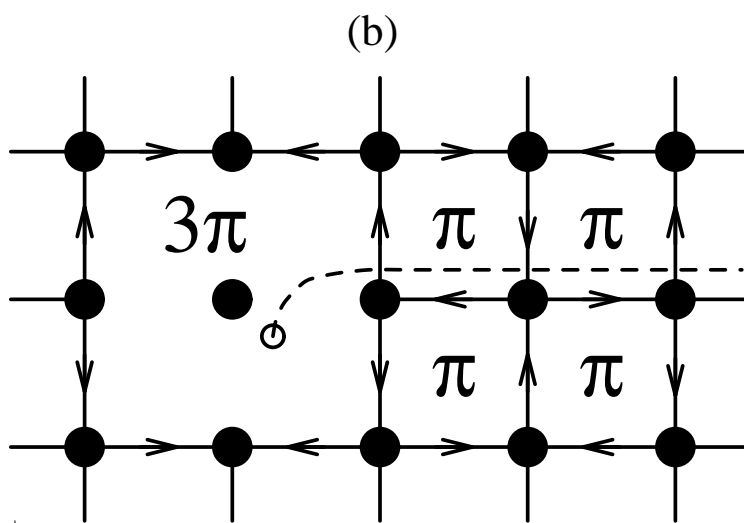
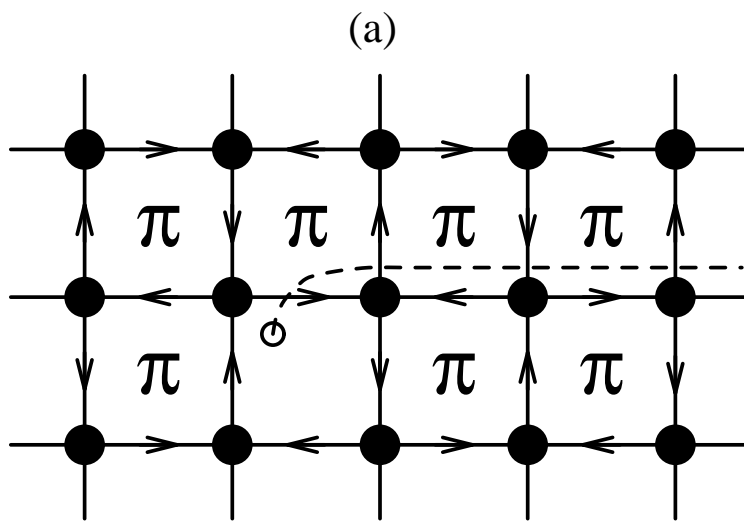
<sup>15</sup> P.W. Anderson, in *Frontiers and Borderlines of Many-particle Physics*, Edited by J.R. Schrieffer, North-Holland ©1987.  
<sup>16</sup> D.S. Rokhsar, Phys. Rev. Lett. **65**, 1506 (1990).  
<sup>17</sup> See, e.g., N. Read and B. Chakraborty, Phys. Rev. B **40**, 7133 (1989).  
<sup>18</sup> Z. Zou and R.B. Laughlin, Phys. Rev. B **42**, 4073 (1990).  
<sup>19</sup> For a similar separation in the context of the quantum Hall effect, see D. Arovas, J.R. Schrieffer, and F. Wilczek, Phys. Rev. Lett. **53**, 722 (1984).  
<sup>20</sup> A phase factor lurking in Eq. (7) must be removed by a trivial phase change to arrive at Eq. (8) with no intrinsic sign. This phase factor is  $g_{ij}/|g_{ij}|$  for the state Eq. (7) with spinons at sites  $i$  and  $j$ , where  $g_{ij} = \langle \chi | c_i^\dagger c_j | \chi \rangle$  is the lattice Green's function in the underlying Slater determinant.  
<sup>21</sup> Note that the phase of  $T_{kij}$  generally has smaller Monte Carlo error bars than the amplitude.  
<sup>22</sup> D.S. Rokhsar, Phys. Rev. Lett. **70**, 493 (1993).  
<sup>23</sup> For an alternate source of nearest-neighbor hole hopping strength enhancement, see J.E. Hirsch and F. Marsiglio, Phys. Rev. B **41**, 2049 (1990).  
<sup>24</sup> To be more precise the modulus of the link variables  $\chi_{ij}$  should not be strictly equal to zero beyond the next-nearest neighbor distance, but should rather decay to zero exponentially in distance. See ref. 18.  
<sup>25</sup> The solutions have to vanish at  $z_A$  and  $z_B$  but this can be taken care of by the function  $g(z)$ .



D.M. Deaven, Figure 3

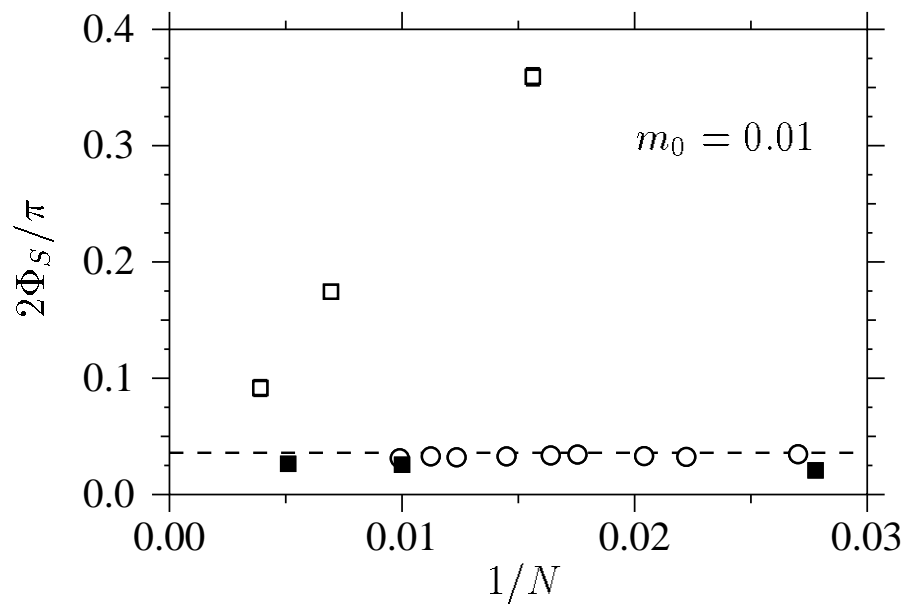


D.M. Deaven, Figure 5

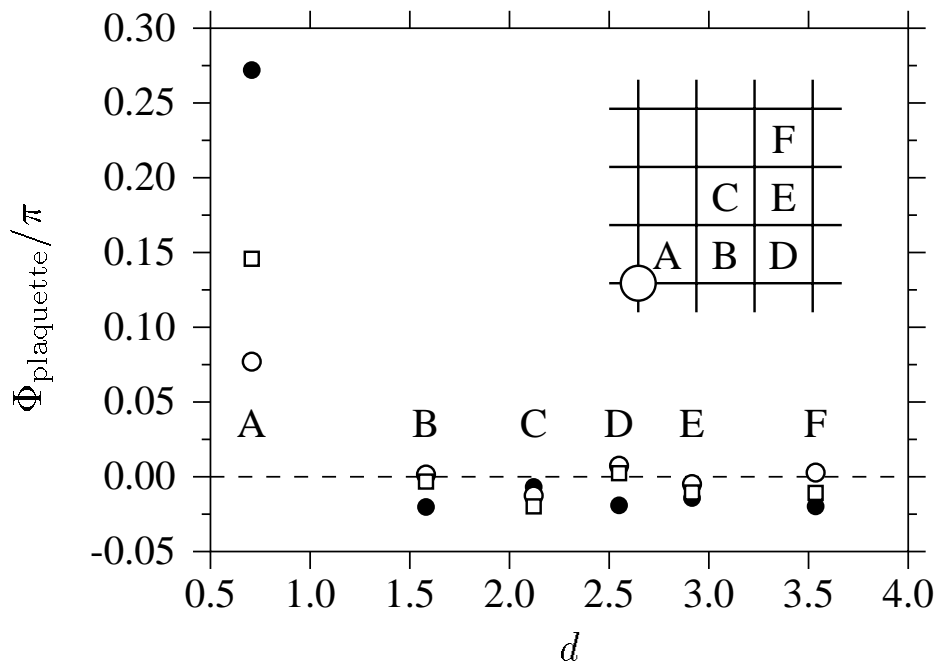


D.M. Deaven, Figure 4



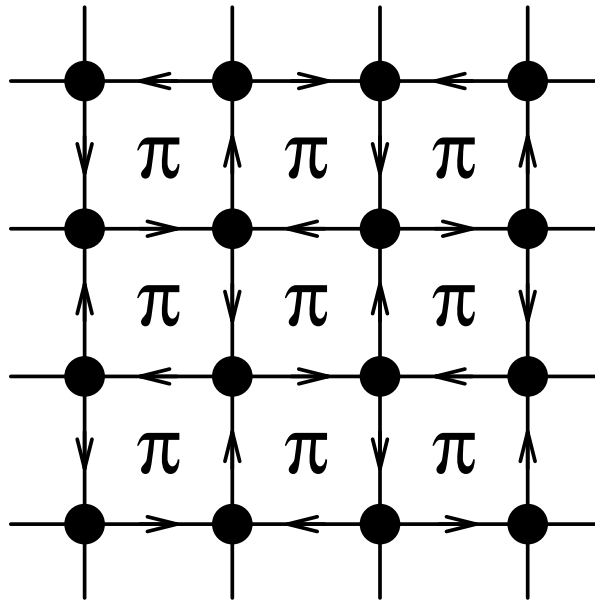


D.M. Deaven, Figure 8

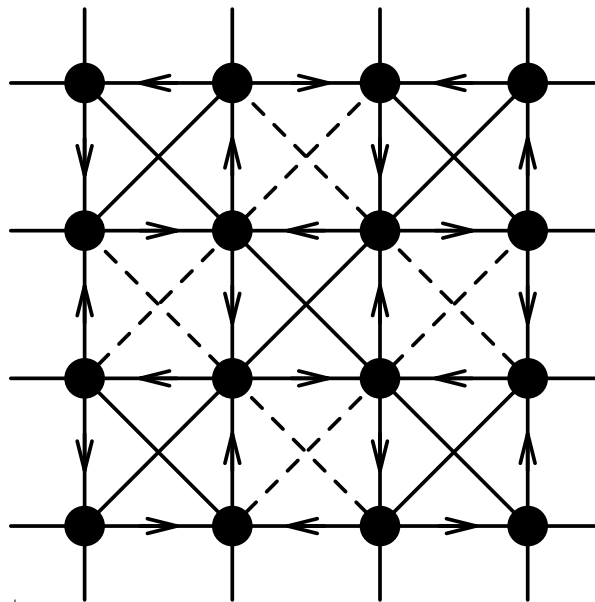


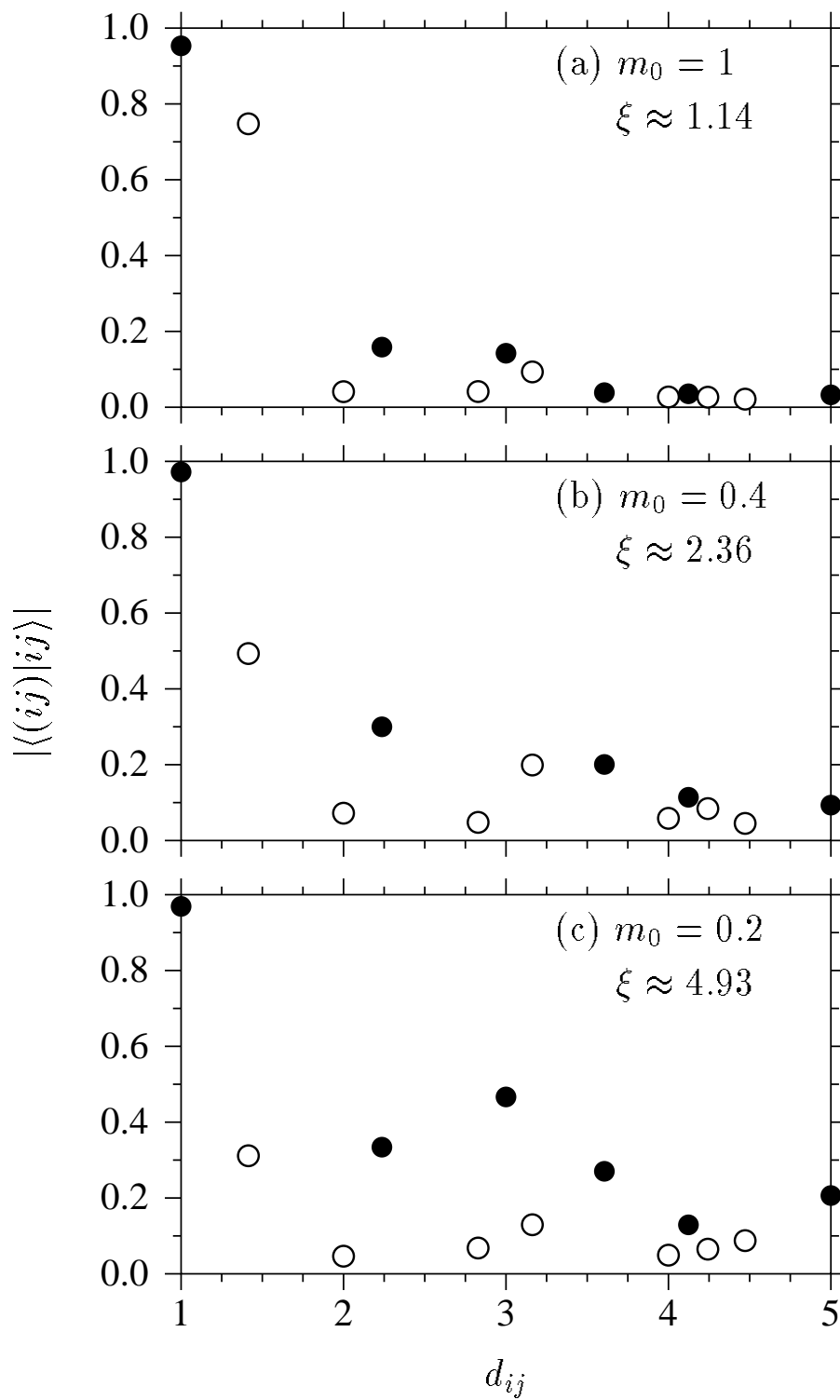
D.M. Deaven, Figure 6

(a)

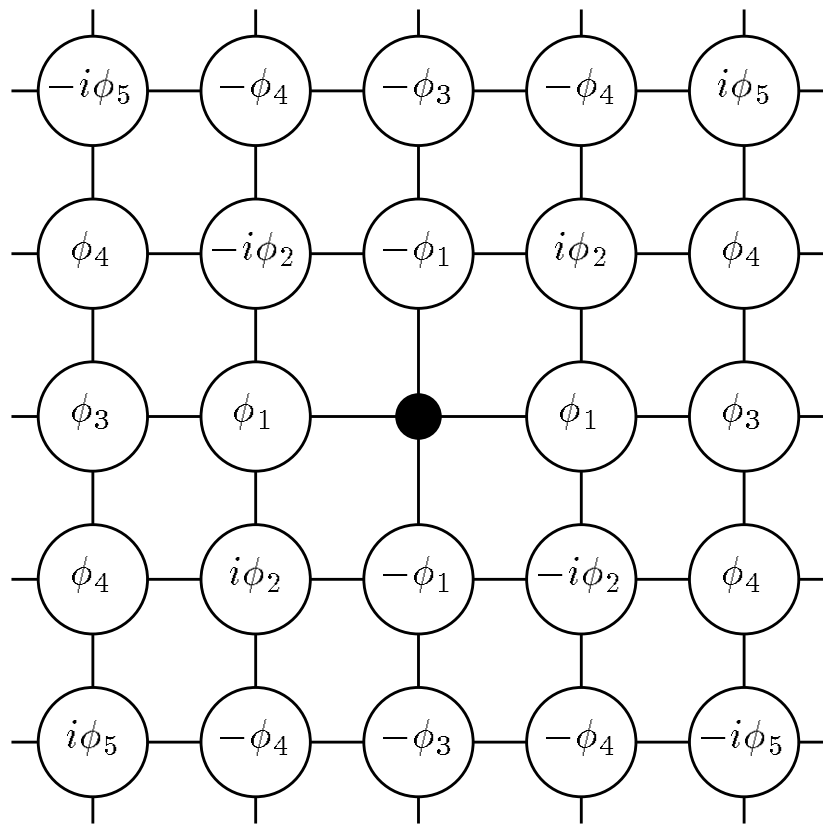


(b)

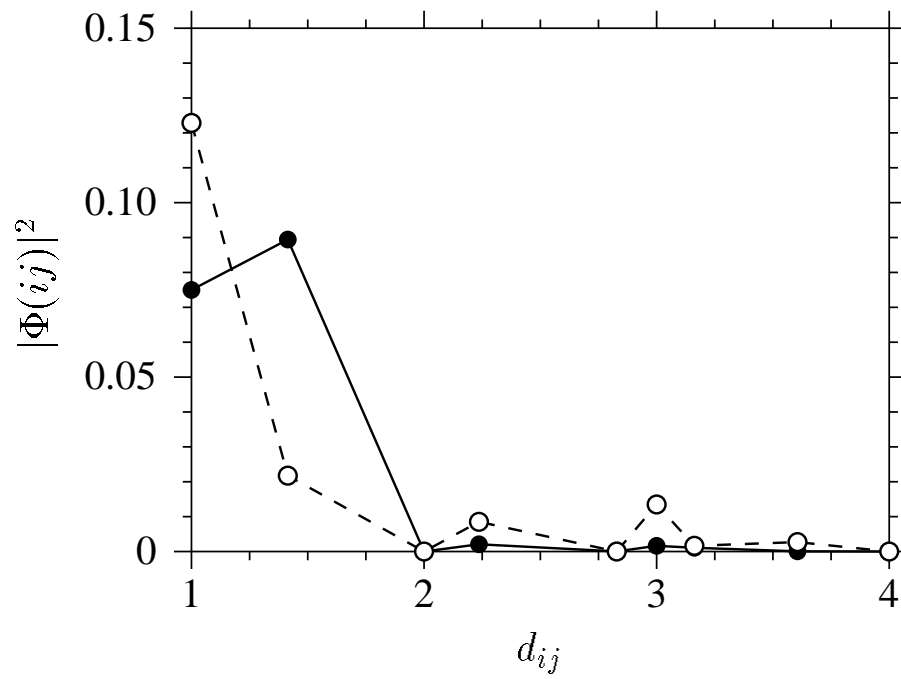




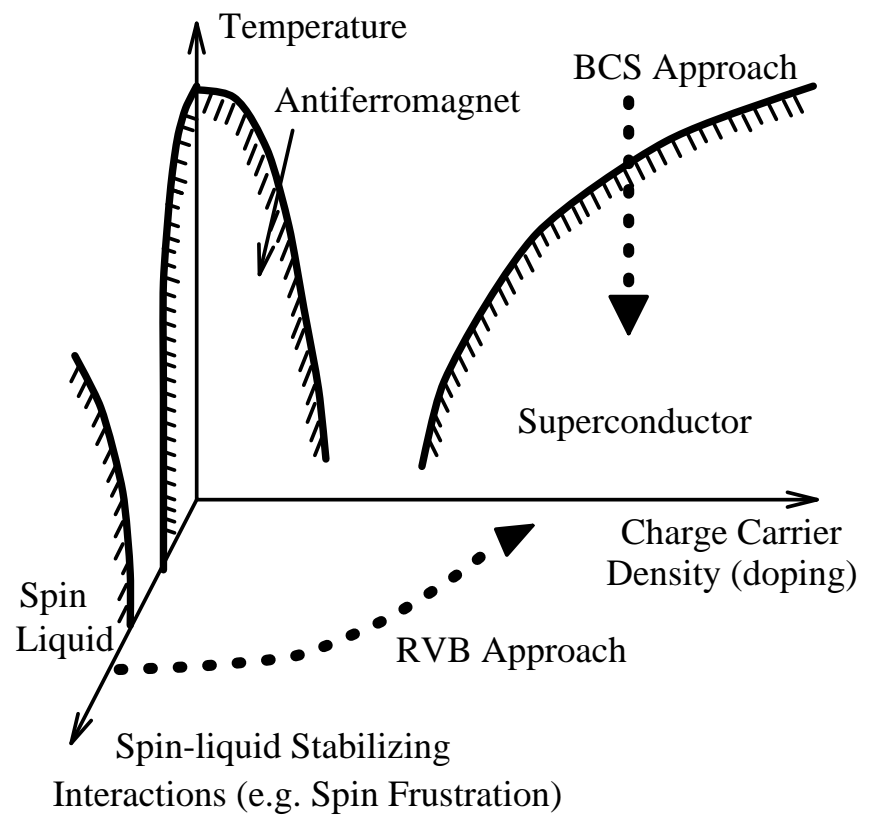
D.M. Deaven, Figure 9



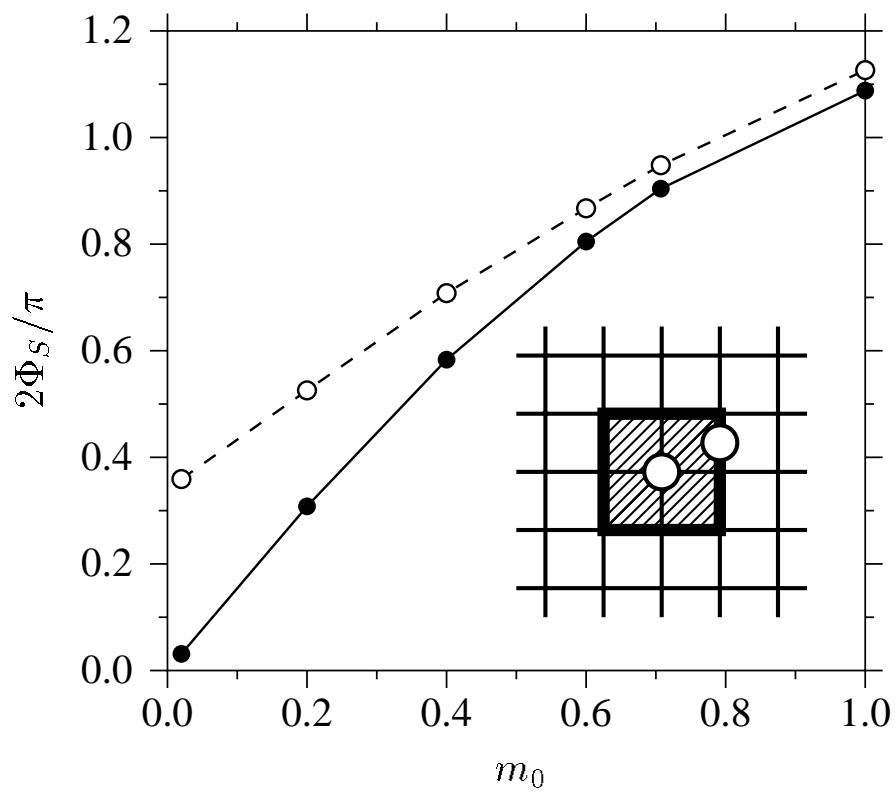
D.M. Deaven, Figure 10



D.M. Deaven, Figure 11



D.M. Deaven, Figure 1



D.M. Deaven, Figure 7